RESEARCH **Open Access**



Construction and characterization of BsGDH-CatIB variants and application as robust and highly active redox cofactor regeneration module for biocatalysis

Kira Küsters^{1,2}, Ronja Saborowski¹, Christian Wagner¹, Rebecca Hamel¹, Jan-Dirk Spöring^{1,3}, Wolfgang Wiechert^{1,4} and Marco Oldiges^{1,2*}

Abstract

Background: Catalytically active inclusion bodies (CatlBs) are known for their easy and cost efficient production, recyclability as well as high stability and provide an alternative purely biological technology for enzyme immobilization. Due to their ability to self-aggregate in a carrier-free, biodegradable form, no further laborious immobilization steps or additional reagents are needed. These advantages put CatlBs in a beneficial position in comparison to traditional immobilization techniques. Recent studies outlined the impact of cooperative effects of the linker and aggregation inducing tag on the activity level of CatlBs, requiring to test many combinations to find the best performing CatlB variant.

Results: Here, we present the formation of 14 glucose dehydrogenase CatlB variants of Bacillus subtilis, a well-known enzyme in biocatalysis due to its capability for substrate coupled regeneration of reduced cofactors with cheap substrate glucose. Nine variants revealed activity, with highest productivity levels for the more rigid PT-Linker combinations. The best performing CatlB, BsGDH-PT-CBDCell, was characterized in more detail including long-term storage at -20 °C as well as NADH cofactor regeneration performance in repetitive batch experiments with CatlB recycling. After freezing, BsGDH-PT-CBDCell CatlB only lost approx. 10% activity after 8 weeks of storage. Moreover, after 11 CatlB recycling cycles in repetitive batch operation 80% of the activity was still present.

Conclusions: This work presents a method for the effective formation of a highly active and long-term stable BsGDH-CatIB as an immobilized enzyme for robust and convenient NADH regeneration.

Keywords: Catalytically active inclusion bodies, Immobilization, Protein aggregates, Protein engineering, Downstream processing, Enzymes

Full list of author information is available at the end of the article

Background

Catalytically active inclusion bodies (CatIBs) can be used as alternative enzyme immobilization strategy with high application potential. In contrast to other enzyme formulations, CatIBs reveal many advantages like low cost production, easy purification and a biologically produced, carrier-free as well as biodegradable immobilization technology without the need for additional carrier



© The Author(s) 2022. Open Access This article is licensed under a Creative Commons Attribution 4.0 International License, which permits use, sharing, adaptation, distribution and reproduction in any medium or format, as long as you give appropriate credit to the original author(s) and the source, provide a link to the Creative Commons licence, and indicate if changes were made. The images or other third party material in this article are included in the article's Creative Commons licence, unless indicated otherwise in a credit line to the material. If material is not included in the article's Creative Commons licence and your intended use is not permitted by statutory regulation or exceeds the permitted use, you will need to obtain permission directly from the copyright holder. To view a copy of this licence, visit http://creativecommons.org/licenses/by/4.0/. The Creative Commons Public Domain Dedication waiver (http://creativeco mmons.org/publicdomain/zero/1.0/) applies to the data made available in this article, unless otherwise stated in a credit line to the data.

^{*}Correspondence: m.oldiges@fz-juelich.de

 $^{^{\}rm 1}$ Institute of Bio- and Geosciences IBG-1: Biotechnology, Forschungszentrum Jülich GmbH, 52425 Jülich, Germany

material or reagents [1-3]. Inclusion bodies (IBs) were long seen as inactive and misfolded protein aggregates. However, for some enzymes the formation of natural CatIBs, like lysine decarboxylase of Escherichia coli (EcLDCc), adenosine 5'-monophosphate phosphorylase of Thermococcus kodakarensis and lipase A of Bacillus subtilis were reported. Instead of inactive inclusion bodies, the protein aggregates retained some catalytical activity [4–6]. Enzymatic activity of such natural CatIBs or of enzymes which do not form any IBs can be enhanced or enforced by generating synthetic tailor-made CatIBs. Different kinds of linker and aggregation inducing tags can be fused to the enzyme of interest to improve the activity of the resulting CatIB. Recent studies revealed that different combinations of linkers and aggregation inducing tags lead to cooperative effects and activity level variations for each specific enzyme. For example, EcLDCc showed higher activity levels in combination with the rigid PT-Linker instead of the flexible SG-Linker [4]. For alcohol dehydrogenase of Ralstonia sp. the combination of the 3HAMP-Tag led to higher k_{cat} values than the TDoT-Tag [7, 8]. Therefore, when testing new enzymes for CatIB formation, a set of different linker/aggregation inducing tag combinations need to be constructed and tested, since systematic structure-function relationship for CatIBs is still to be explored.

Glucose dehydrogenase of Bacillus subtilis (BsGDH, EC 1.1.1.47) can be used to convert β-D-glucose to β-D-glucono-1,5-lactone. During this reaction BsGDH reduces the oxidized cofactor NAD+ to its reduced form NADH [9], which is of high value as reducing reagent for biocatalytic transformations. Therefore, BsGDH can be used as an in-situ cofactor regeneration system, which is essential for industrial application, in order to perform low-cost cofactor recycling of NADH. The use of glucose (0.3 € kg⁻¹) as a substrate is much more cost-efficient than using NADH (184 k \in kg⁻¹) in equimolar amounts. So far, NADH regeneration was performed with the soluble form of GDH, co-immobilized in a nanofiltration membrane reactor or in form of self-assembling allenzyme hydrogels [10-12]. The use of CatIBs for NADH recycling provides an efficient alternative solution showing cost effective production and further advantages, such as long-term storage options, high enzyme stability and simple reusability in repetitive process applications [1], making them the perfect candidates to investigate a novel approach for NADH regeneration in repetitive process application.

Here we report the construction and characterization of a set of *Bs*GDH-CatIB variants. The plasmids encoding the CatIBs were generated via Golden Gate Assembly with a set of two linkers and eight aggregation inducing tags. While two combinations failed in the molecular

biology construction, fourteen variants were successfully constructed and characterized regarding morphology and specific volumetric productivity. The best performing CatIB, BsGDH-PT-CBDCell, was characterized in more detail including long-term storage at -20 °C as well as NADH cofactor regeneration performance in repetitive batch experiments with CatIB recycling.

Results and discussion

Production of CatlBs and microscopic analysis

The glucose dehydrogenase of Bacillus subtilis (BsGDH; EC 1.1.1.47), was C-terminally fused with either a flexible SG- or a more rigid PT-Linker as well as one out of eight aggregation inducing tags (TDoT, 18AWT, L6KD, GFIL8, 3HAMP, TorA, CBDCell and ELK16; see Additional file 1: Table S1) [1, 6, 13-19]. BsGDH has a homotetrameric quaternary structure with free C- and N-termini. In this study, the 16 possible linker/aggregation inducing tag combinations were fused to the C-terminus of the BsGDH and tested for enzymatic activity. Fourteen BsGDH-CatIB variants were successfully generated and analyzed in more detail. The fourteen CatIB variants were produced in E. coli BL21(DE3) using M9 autoinduction medium (See Additional file 1: Table S2). Phase contrast microscopy with a 1000-fold magnification was used to verify the formation of BsGDH-CatIBs in this host (see Methods). Like typical IBs, CatIBs can be found at the cell poles as granule-like structures or refractive particles (Fig. 1) [20]. All strains were screened via microscopic analysis to observe the CatIB formation and the influence on the cell and CatIB morphology.

The microscopic analysis of the BsGDH-CatIB variants confirmed the hypothesis that combinations of different linkers and aggregation inducing tags lead to different cell and IB morphologies [4]. The variants with PT-L6KD and SG-ELK16 formed dense inclusion bodies with 63% and 75% of the cells carrying CatIBs, respectively (Fig. 1, Table 1). Whereas the cells with SG-ELK16 revealed an E. coli like cell structure, the cells carrying the CatIB with PT-L6KD appeared in an untypically round cell structure. Very similar IB and cell morphologies were found with both linkers and aggregation inducing tags, but the overall yield of cells carrying CatIBs showed large differences. While for CBDCell (SG: 75%; PT: 78%) and GFIL8 (SG: 63%; PT: 75%) more than 50% of the cells showed CatIBs, TorA (SG: 32%; PT: 23%), TDoT (SG: 17%; PT: 13%) and 3HAMP (SG: 16%; PT: 6%) resulted in values from 6 to 32% only. Whilst PT-18AWT did not form any IBs, the corresponding SG-18AWT variant displayed only 1% IB carrying cells. Interestingly, the same phenomenon was shown for the 18AWT-Tag with EcLDCc and strengthened the hypothesis that this tag has a higher tendency to bind to cell membrane components

Küsters et al. Microbial Cell Factories (2022) 21:108 Page 3 of 10

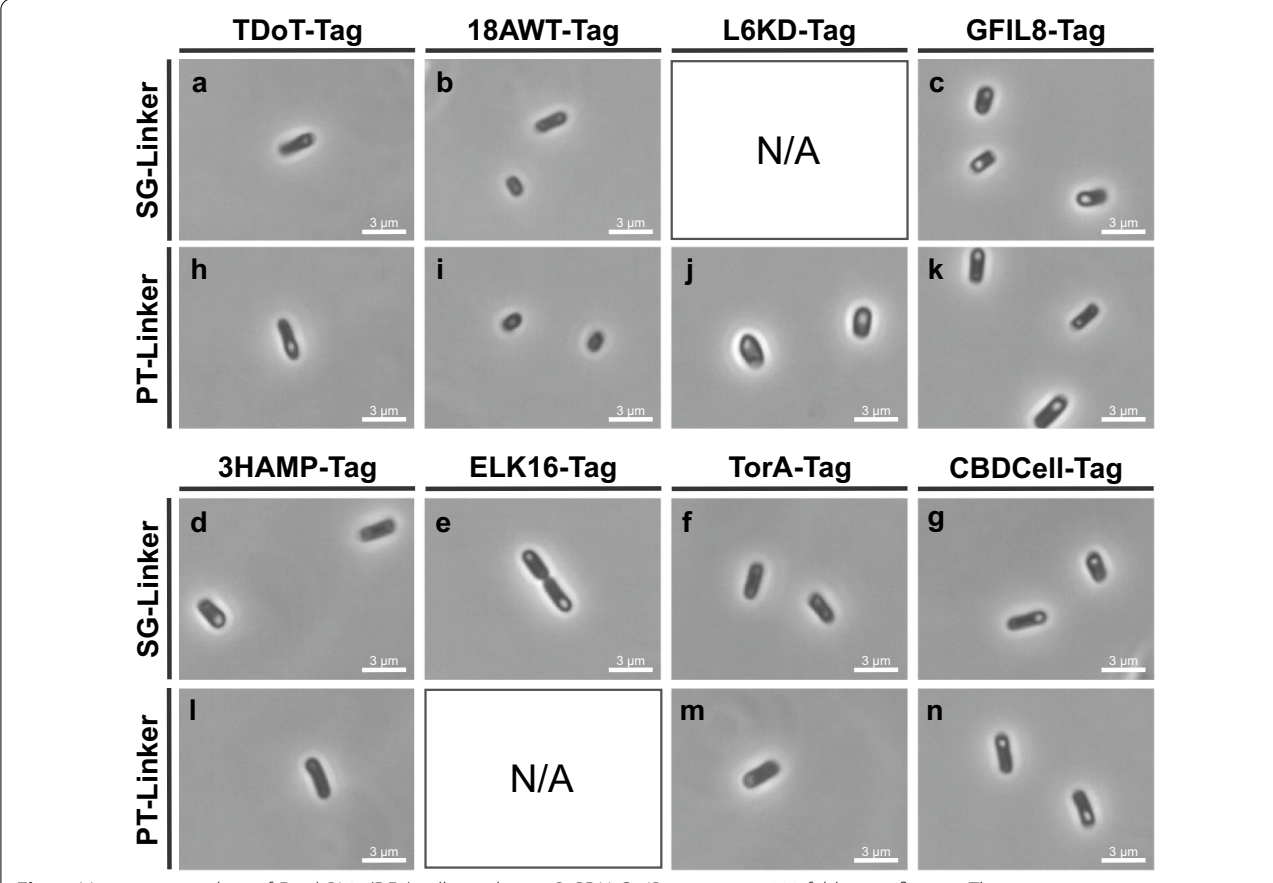


Fig. 1 Microscopic analysis of *E. coli* BL21(DE3) cells producing *Bs*GDH-CatlB variants at 1000-fold magnification. The microscopic images were taken after cultivation for 3 h at 37 °C followed by 69 h at 15 °C in M9-Al. **a** *Bs*GDH-SG-TDoT, **b** *Bs*GDH-SG-18AWT, **c** *Bs*GDH-SG-GFIL8, **d** *Bs*GDH-SG-3HAMP, **e** *Bs*GDH-SG-ELK16, **f** *Bs*GDH-SG-TorA, **g** *Bs*GDH-SG-CBDCell, **h** *Bs*GDH-PT-TDoT, **i** *Bs*GDH-PT-18AWT, **j** *Bs*GDH-PT-L6KD, **k** *Bs*GDH-PT-GFIL8, **l** *Bs*GDH-PT-3HAMP, **m** *Bs*GDH-PT-TorA, **n** *Bs*GDH-PT-CBDCell

rather than forming isolated IBs [4, 21]. Moreover, comparing microscopic analysis data of *Bs*GDH with previous results from *Ec*LDCc revealed similar CatIB and cell morphology effects, such as abnormal cell structures in combination with L6KD-Tag or a looser CatIB structure with 3HAMP-Tag, but it is less dominant with *Bs*GDH than with *Ec*LDCc. Strikingly, the influence of the linker/aggregation inducing tag combination on CatIB formation was different between the two enzymes. With *Ec*LDCc-SG-TDoT 78% of the cells carried CatIBs, whereas with *Bs*GDH-SG-TDoT it was only 17% [4]. This strongly supports the hypothesis that there is no optimal linker/aggregation inducing tag combination, but rather a more complex interaction between the three parts, i.e., including the nature of the target protein in focus.

Downstream processing and specific volumetric productivity of fourteen BsGDH-CatlB variants

A high overall protein yield together with high enzymatic activity are important CatIB features. A previously

improved purification protocol [4] was used for simple and fast CatIB purification. The purified CatIBs were divided in several identical 1 mL aliquots. Three of these aliquots were used for the CatIB weight determination and one or three others were used for activity measurement. Moreover, presence of CatIBs was verified via sodium dodecyl sulfate- polyacrylamide gel electrophoresis (SDS-PAGE, Additional file 1: Figure S1). The SDS gel revealed respective bands for all *Bs*GDH-CatIB variants in the insoluble pellet fraction, except for the variants with PT-18AWT, PT-TorA and SG-TorA (Table 1).

After CatIB purification and SDS-PAGE analysis, an enzymatic activity assay was performed in 40 mM TAE buffer (pH 7) using 200 mM glucose as a substrate and 0.4 mM NAD⁺ as the cofactor. The reproducibility of the CatIB purification and enzyme assay workflow was tested in technical triplicates with *Bs*GDH-PT-CBDCell and *Bs*GDH-SG-ELK16 (Fig. 2). The other CatIB variants have been tested in analytical triplicates. In general, a sufficiently good reproducibility of the technical and

Küsters et al. Microbial Cell Factories (2022) 21:108 Page 4 of 10

Table 1 Protein production and productivity data of BsGDH wild type and BsGDH-CatlB variants

	CatlBs visibility (SDS) (Yes/No)	CatlBs visibility (Microscopy) (Yes/ No)	Cells with CatlBs [%]	Pellet activity (Yes/No)	P _v Pellet (g L ⁻¹ d ⁻¹)	Specific P _v Pellet (g L ⁻¹ d ⁻¹ g _{CatlB} ⁻¹)	P _v Supernatant (g L ⁻¹ d ⁻¹)
BsGDH _{WT}	No	No	0	No	0	0	76.8
BsGDH-PT-TorA	No	No	0	No	0	0	1.9
BsGDH-PT-CBDCell	Yes	Yes	52	Yes	19.0	55.8	0.3
BsGDH-PT-3HAMP	Yes	Yes	6	Yes	12.6	48.3	0.8
BsGDH-PT-GFIL8	Yes	Yes	75	Yes	6.7	26.8	1.3
BsGDH-PT-L6KD	Yes	Yes	63	Yes	19.6	36.3	5.4
BsGDH-PT-18AWT	No	No	0	No	0	0	11.3
BsGDH-PT-TDoT	Yes	Yes	13	Yes	16.3	24.3	11.3
BsGDH-SG-ELK16	Yes	Yes	75	Yes	2.3	7.9	0
BsGDH-SG-TorA	No	Yes	32	No	0	0	24.7
BsGDH-SG-CBDCell	Yes	Yes	75	Yes	0.6	2.6	0
BsGDH-SG-3HAMP	Yes	Yes	16	Yes	1.0	3.2	3.6
BsGDH-SG-GFIL8	Yes	Yes	63	No	0	0	0
BsGDH-SG-18AWT	Yes	Yes	79	No	0	0	1.3
BsGDH-SG-TDoT	No	No	0	Yes	1.4	6.4	11.2

Pellet activity was tested by adding 200 mM glucose, 0.4 mM NAD⁺ and 40 mM TAE buffer (pH 7) to the CatlB pellet fraction after purification. Productivity was calculated after 20 min (pellet fraction), 12 min (supernatant; BsGDH-CatlBs) or 6 min (supernatant BsGDH_{WT}) reaction time. Microscopic images were taken after main cultivation (72 h) and analyzed regarding the number of cells that carry CatlBs (n \geq 45).

 P_V : volumetric productivity ($g_{NADH} L^{-1} d^{-1} g_{CatlB}^{-1}$)

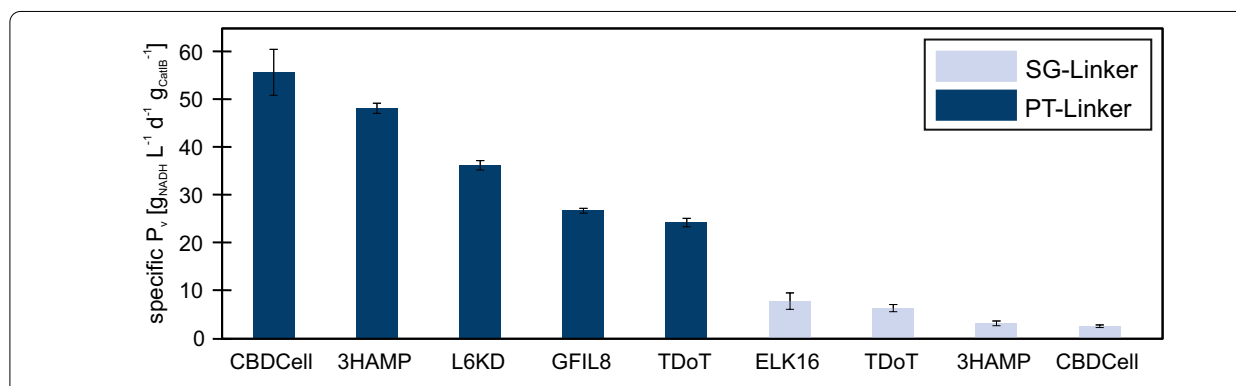


Fig. 2 Comparison of specific volumetric productivity of fourteen BsGDH-CatlBs. The enzyme assay was performed at 37 °C, 15 min, 1000 rpm, 1 mL in 40 mM TAE buffer (pH 7) with 200 mM glucose and 0.4 mM NAD⁺. CatlB weight was determined after drying the CatlBs at 80 °C for 24 h, followed by additional 24 h in a desiccator. n_t = 3 for PT-CBDCell and SG-ELK16; all others: n_a = 3

analytical replicates was observed with relative standard deviation of 8.6–21.8% and 2.2–15.4%, respectively. The errors of the technical replicates were found to be slightly higher, since they include the pure analytical error as well the pipetting and processing steps. The specific volumetric productivity (specific $P_{\rm v}$) of all variants was determined based on NADH conversion after 20 min reaction time. A comparison of the specific $P_{\rm v}$ showed that nine out of the fourteen CatIB variants revealed activity, with the 18AWT- and TorA-Tag with both linkers and the GFIL8-Tag with PT-linker showing no activity. Strikingly,

the five highest specific P_v values were all reached with the more rigid PT-Linker combinations. This strengthens the hypothesis from Küsters et al. 2021 that the linker selection has an enormous impact on the CatIB performance as indicated by the PT-Linker leading to higher specific P_v values with the BsGDH-CatIB data. The rigidity of the PT-Linker seems to have an important influence on the CatIB structure–function relationship. However, although the PT-Linker again led to higher productivity, the ranking of the best aggregation inducing tags differed between the two enzymes. Interestingly, only a few cells

with *Bs*GDH-PT-3HAMP formed visible CatIBs (6%), but this variant is the second best CatIB variant in specific P_v. This indicates that 3HAMP seems to favor more loose CatIB structures, which were not fully visible under the microscope. This effect was already shown in [19] where a combination with 3HAMP resulted in high activity levels for benzaldehyde lyase from *Pseudomonas fluorescens*, but without revealing visible CatIBs in light microscopy.

Enzymatic activity vs morphology of BsGDH-CatIB variants

The comparison of CatIB visibility on microscope pictures as well as on SDS gels with the productivity levels of the CatIBs revealed suitable and less suitable BsGDH-CatIBs. Contrary to a few other enzymes, the control, BsGDH wild type, did not form natural CatIBs [4-6]. Despite being highly expressed from the same plasmid construct as the CatIB variants, it seems that the wild type enzyme showed a typical soluble protein behavior which is given by: (I) no insoluble fragment on SDS gel, (II) no visible IBs on microscopic images, (III) no activity in the pellet fraction after purification and (IV) activity in the supernatant (76.8 $g_{NADH} L^{-1} d^{-1}$). The CatIB variants showed clear differences between the linker/aggregation inducing tag combinations. The two aggregation inducing tags, TorA and 18AWT, only formed inactive IBs. Only SG-18AWT revealed a band in the insoluble fraction of the SDS gel, meaning that the other variants did not form insoluble protein or the level was too low to be verified via SDS-PAGE. In case of TorA, the formation of visible CatIBs was proven with microscopic images (PT: 23% and SG: 32%). However, it may happen that these insoluble proteins return to their soluble form during the purification procedure. This hypothesis might be strengthened by the fact that the supernatant after cell lysis of BsGDH-SG-TorA has the highest productivity level (24.7 $\rm g_{NADH}~L^{-1}~d^{-1})$ of all CatlBs. Moreover, BsGDH-SG-GFIL8 did not reveal any pellet activity, which made this variant together with 18AWT and TorA variants irrelevant for further analysis. In comparison to these inactive variants, nine of fourteen variants revealed enzymatic activity in the pellet fraction. The productivity level differed between the variants from 2.6 g_{NADH} L⁻¹ d⁻¹ g_{CatlB} -1 (*Bs*GDH-SG-CBDCell) up to 55.8 g_{NADH} L⁻¹ d⁻¹ g_{CatlB} -1 (*Bs*GDH-PT-CBDCell). A previous study showed that EcLDCc in combination with the PT-L6KD showed the highest activity whereas the combination with SG-Linker showed the lowest activity [4]. The same effect was shown for BsGDH-CatIBs, where SG-CBDCell revealed the lowest productivity level and BsGDH-PT-CBDCell the highest. Moreover, BsGDH-PT-CBDCell was also the variant that revealed the highest number of CatIB producing cells (78%). Nevertheless, the comparative analysis of microscopic image data and activity of all variants showed that a high number of CatIB forming cells alone is not predictive of high activity levels. For example $Bs\mathrm{GDH}$ in combination with PT-GFIL8, SG-ELK16 and SG-CBD-Cell all revealed 75% CatIB producing cells. However, the productivity levels of these CatIB variants differed between 26.8 g_{NADH} L $^{-1}$ d $^{-1}$ g_{CatIB} $^{-1}$ ($Bs\mathrm{GDH}$ -PT-GFIL8), 7.9 g_{NADH} L $^{-1}$ d $^{-1}$ g_{CatIB} $^{-1}$ ($Bs\mathrm{GDH}$ -SG-ELK16) and 2.6 g_{NADH} L $^{-1}$ d $^{-1}$ g_{CatIB} $^{-1}$ ($Bs\mathrm{GDH}$ -SG-CBDCell). Taking all together, the most important results were (I) variants without visible CatIBs on microscopic images and on SDS gel can be excluded from further analysis, (II) microscopic images alone cannot be used to confirm successful CatIB formation, (III) the linker is one decisive factor for high activity and (IV) $Bs\mathrm{GDH}$ -PT-CBDCell is the best performing CatIB for $Bs\mathrm{GDH}$.

CatlB storage condition test with BsGDH-PT-CBDCell

The best BsGDH-CatIB, BsGDH-PT-CBDCell, was used to characterize potentially suitable long-term storage conditions. In previous studies, lyophilization of CatIBs was used for long-term storage [1, 7, 13]. In this study, the long-term storage of lyophilized pellets (LP) and wet pellets (WP) was compared. Whereas WP were directly stored at -20 °C, LP were first lyophilized (Fig. 3). A reference assay was performed immediately after purification at the same day (day 0) to visualize the activity loss of the CatIB due to initial freezing and lyophilizing step. This reference value was set to 100%. After storing WP and LP at -20 °C for 9, 17, 31, 39, 44 and 56 days, the CatIBs were tested for their activity. Whereas the WP showed an initial loss of approx. 40%, LP revealed an initial loss in the range of about 60% in comparison to the non-frozen reference sample at day 0 directly after purification. Interestingly, in the LP and WP samples from day 9 to 56, there is no clear trend to lower activity values, indicating that the first step of lyophilisation or freezing is the most harmful step. It seemed that freezing the WP directly without lyophilization led to higher remaining activity of the CatIB and lyophilization did not show a positive effect during the investigated time frame. Apart from the loss of activity due to the treatment before -20 °C storage, both methods led to stable CatIB activity levels over the entire time span. In contrast to the BsGDH-CatIB data, a hydroxynitrile lyase CatIB of Arabidopsis thaliana revealed higher activity levels when using it in lyophilized form [13]. This indicated that the best storage condition could also differ between various CatIB enzymes.

CatlB and NADH recycling with BsGDH-PT-CBDCell

Based on the promising results from previous experiments, the best CatIB candidate, *Bs*GDH-PT-CBDCell,

Küsters et al. Microbial Cell Factories (2022) 21:108 Page 6 of 10

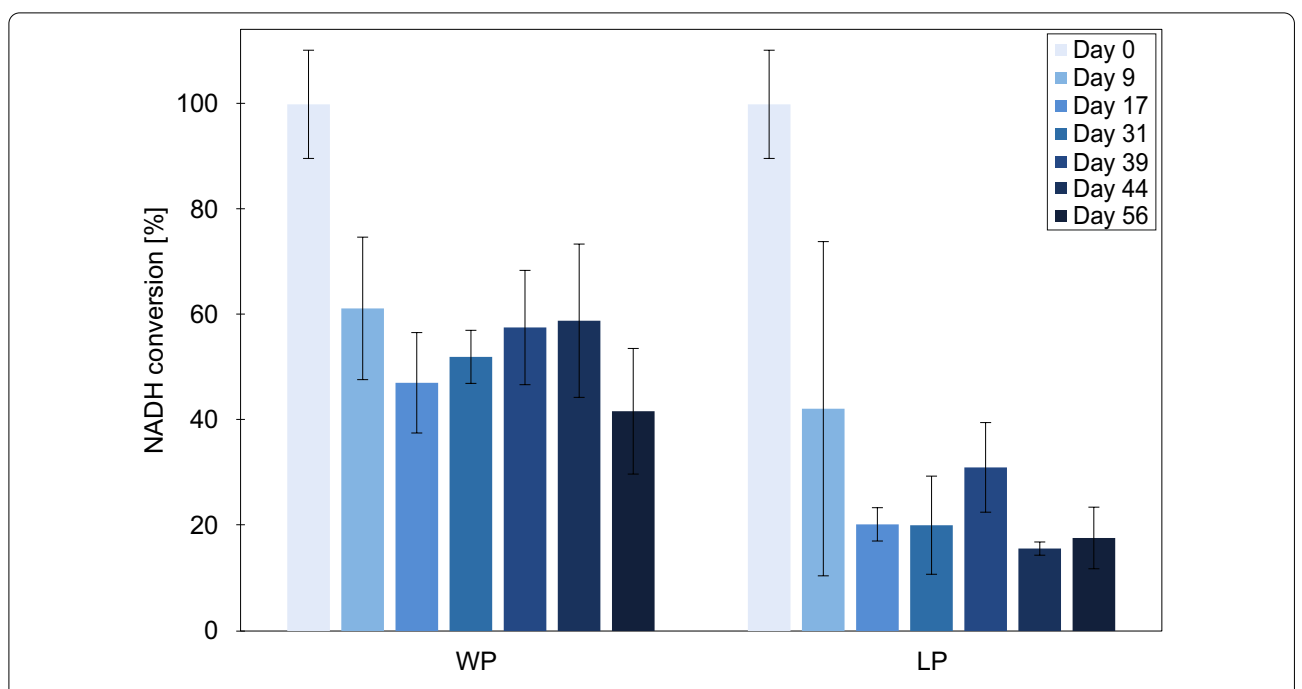


Fig. 3 Storage stability testing of BsGDH-PT-CBDCell. The wet pellets (WP) were directly frozen after purification or first lyophilized (LP) before storing them in the freezer at -20 °C. Technical triplicates were tested. The enzyme assays were performed at 37 °C, 15 min, 1000 rpm, 1 mL in 40 mM TAE buffer (pH 7) with 200 mM glucose and 0.4 mM NAD⁺. A reference assay was performed at day 0, before freezing or freeze-drying. The other assays were performed at day 9, 17, 31, 39, 44 and 56

was also used to test the stability and robustness during repetitive batch process application. This nicely showcased the (I) biocatalytic performance of the BsGDH-CatIB to efficiently regenerate NADH from its oxidized form NAD+ and (II) the high stability of the CatIB variant during recycling in repetitive batch process. For this, propanal reduction with NADH to propanol catalyzed by the alcohol dehydrogenase from Saccharomyces cerevisiae (ScADH) was coupled with NADH cofactor regeneration enabled by BsGDH-PT-CBDCell CatIB oxidation of glucose to gluconate. To set up the repetitive batch on a 0.5 mL scale, 200 mM glucose, 0.4 mM NAD+, 20 mM propanal, and 11.5 U ScADH was used. Each of the eleven repetitive batch cycles was performed with the recycled CatIBs for 30 min. For the glucose/propanal ratio a tenfold excess of glucose was chosen. In order to avoid any issue with propanal substrate volatility, it was used at 20 mM, which was approx. 4 times higher than the expected conversion to the product propanol. Reaction monitoring of the biocatalytic process was done by gas chromatography measurement of the propanol concentration (Fig. 4a) and spectrophotometric measurement of the NADH concentration (Fig. 4b).

The repetitive batch experiment revealed the cooperative activity of the *Bs*GDH-PT-CBDCell CatIB and the *Sc*ADH, as shown by the formation of propanol (Fig. 4a;

GDH+ADH). The control experiments with BsGDH-PT-CBDCell CatIB and ScADH alone did not show any propanol. This was expected since in the case of ScADH only NAD+ is provided and no NADH is present here. For the sole use of BsGDH-PT-CBDCell CatIB no propanol formation was found, due to the lack of ScADH. Nevertheless, BsGDH-PT-CBDCell CatIB activity could be verified in the controls proven by NADH concentration in the range of approx. 0.4 mM which was formed from the NAD⁺ present (Fig. 4b; GDH only). Interestingly, the data for propanol and NADH concentration were slightly increasing during the first 4 cycles (Fig. 4a, b). This effect may have occurred because of already bound NAD+ in the reused BsGDH-CatIBs or some activation effect during the initial cycles. The experiments with BsGDH-PT-CBDCell CatIB to regenerate NADH from NAD+ and the ScADH show the biocatalytic reaction from propanal to propanol with in-situ regeneration of reduced cofactor NADH. Interestingly, the NADH level stays low during the whole reaction time, indicating that the NADH regeneration was the rate limiting step in the reaction sequence and that overall reaction was not completed. This is supported by the estimation of overall propanal conversion to be approx. 15-20% based on 20 mM initial propanal substrate concentration and about 3-4 mM propanol product after each 30 min reaction cycle. As

Küsters et al. Microbial Cell Factories (2022) 21:108 Page 7 of 10

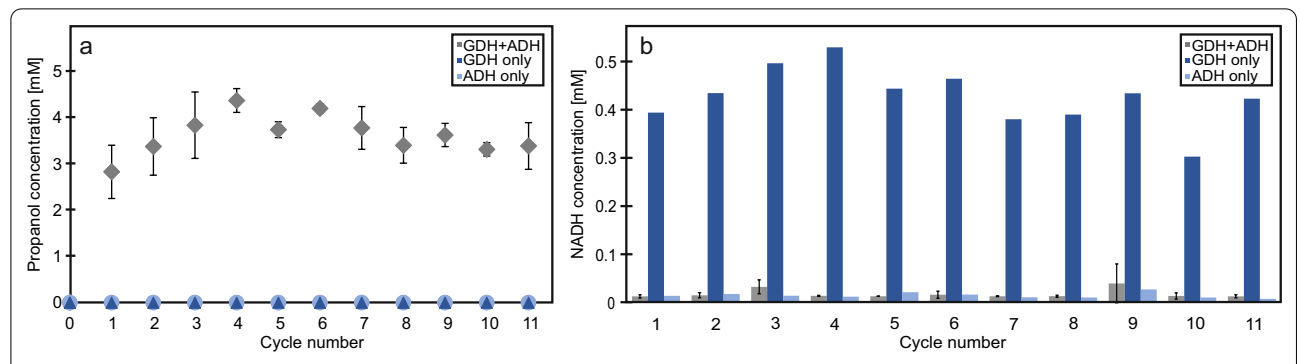


Fig. 4 Repetitive batches for the production of propanol from propanal with soluble *Sc*ADH and *Bs*GDH-CatlBs for NADH recycling. **a** Measured propanal concentration with GC. **b** NADH concentration was measured with a photometer. *Bs*GDH-CatlBs, purified from 0.5 mL cells with OD_{600nm} 20, were reused for 11 cycles. 11.5 U *Sc*ADH were freshly added with 40 mM TAE (pH 7), 200 mM glucose, 20 mM propanal, 0.4 mM NAD in each cycle. The final reaction volume was 0.5 mL. Each reaction was performed at 37 °C for 30 min. GDH + ADH samples were measured in technical triplicates

a consequence based on 0.4 mM initial NAD+concentration, each cofactor molecule was regenerated approx. 7.5–10 times. In order to optimize the biocatalytic reaction more BsGDH-PT-CBDCell CatIB could be used in order to increase the regeneration rate of NADH and initial NAD+might be also reduced. Since there is simple access to BsGDH-PT-CBDCell CatIB preparations with option for stable long term storage at -20 °C for at least 8 weeks, this seems to be a convenient and readyto-use NADH cofactor regeneration module for biocatalytic conversions. The data of the eleven repetitive batch processes seem to indicate highly stable NADH regeneration enabled by the BsGDH-PT-CBDCell CatIBs and one could speculate that many more reaction cycles would have been possible. Moreover, the aliquots of the lyophilized or directly frozen CatIB preparations could be added during the process, in case enzymatic activity needs to be increased or if a specific limiting NADH regeneration rate should be realized.

Conclusion

Although microscopic and SDS-PAGE analysis alone cannot be used to make predictions about the CatIB productivity levels, these methods are important tools to do a pre-sorting of successful CatIB generation, especially when analyzing many CatIB variants in a short time. Strains without any visible IBs on the microscopic images in combination with missing bands in the insoluble fraction on the SDS gel can be directly excluded from further analysis to save resources and time.

Nine out of fourteen *Bs*GDH-CatIBs revealed glucose dehydrogenase activity. The most efficient *Bs*GDH CatIB was *Bs*GDH-PT-CBDCell showing effective CatIB formation in 78% of the *E. coli* cells in combination with the

highest specific P_v value (55.8 g_{NADH} L^{-1} d^{-1} g_{CatlB}^{-1}). As mentioned in previous studies, the more rigid PT-Linker led to higher specific P_v values than the SG-Linker, which strengthened the hypothesis that the linker has a decisive influence on the CatlB activity [4]. Nevertheless, it was also shown that the aggregation inducing tag has a significant influence on the activity, which seems to strictly depend on the enzyme used. These results indicate, when generating CatlBs with new proteins of interest, many linker/aggregation inducing tag combination needs to be tested to find not only successful CatlB variants with some enzymatic activity, but linker/aggregation inducing tag combinations with high performance applicable for robust biocatalytic processes.

Additionally, *Bs*GDH-PT-CBDCell CatIBs showed a high long-term storage stability at -20 °C and also high stability in solution, as has been demonstrated in repetitive batch experiments for NADH recycling with commercial *Sc*ADH.

In comparison to traditional GDH technologies, like using soluble or immobilized enzyme, which can either be used only once or several times requiring additional immobilization or filtration steps, $Bs{\rm GDH\text{-}CatIBs}$ enable a simple self-immobilization technology in combination with convenient reusability with high rates. The achieved NADH regeneration rates in the range of 2 ${\rm g}_{\rm NADH}$ L $^{-1}$ h $^{-1}$ ${\rm g}_{\rm CatIB}^{-1}$ provide attractive performance. With these features, especially $Bs{\rm GDH\text{-}PT\text{-}CBDCell}$ would be suitable as a NADH regeneration module in future biocatalytic research and industrial application.

Methods

Reagents and chemicals

All chemicals were purchased from ROTH (Karlsruhe, Germany) and Merck (Sigma-Aldrich, Missouri, USA),

unless stated otherwise. Enzymes for molecular biology were purchased from New England Biolabs GmbH (Frankfurt am Main, Germany).

Construction of expression plasmids

The synthetic gene of the BsGDH, the SG- and PT-Linker as well as the eight aggregation inducing tags, TDoT-, 18AWT-, L6KD-, GFIL8-, 3HAMP-, TorA-, CBDCell-, ELK16-Tag, were synthesized by Synbio Technologies (Monmouth Junction, New Jersey, USA). The synthetic sequences contained BsaI recognition and restriction sites needed for Golden Gate Assembly. The synthetic gene encoding for BsGDH was assembled with one of the two linkers, one of the eight aggregation inducing tags as well as the so-called suicide plasmid in a ratio of 1:1:1:3 during Golden Gate Assembly. The suicide plasmid served as the expression plasmid backbone. It consisted of a pET28a vector with an integrated ccdB gene, coding for the CcdB toxin, which is lethal for standard E. coli strains, like E. coli DH5α and E. coli BL21(DE3). It functioned as an accurate Golden Gate Assembly control with zero-background cloning [22]. During Golden Gate Assembly, the ccdB gene was removed by BsaI and the CatIB-Linker-Tag sequence was inserted by the T4-Ligase. After *E. coli* DH5α was transformed with the Golden Gate Assembly mixture, only strains carrying the successful CatIB plasmid were able to grow while strains carrying the original vector were killed due to the produced toxin. To start Golden Gate Assembly, 2.5% (v/v) T4-Ligase as well as 2.5% (v/v) BsaI restriction enzyme, was added to the mixture. The Golden Gate Assembly was performed in a PCR cycler (37 °C, 5 min and 16 °C, 5 min-15 cycles; 65 °C, 20 min). Information about all plasmids that were used in this study are summarized in Additional file 1: Table S1, Supporting Information. The final expression plasmids were sequenced and verified for the correct assembly (Eurofins GmbH, Hamburg, Germany).

Protein production, cell disruption and protein purification

CatIB production was performed by cultivating *E. coli* BL21(DE3) carrying the respective expression plasmids in M9 autoinduction medium (See Additional file 1: Table S2). The cultivation was performed after a modified protocol by Lamm et al. 2020, 1 L shaking flasks were used with a filling volume of 100 mL and a shaking frequency of 170 rpm (Infors HT Multitron Standard, Infors AG, Bottmingen, Switzerland). The main cultivation was inoculated with an ${\rm OD_{600nm}}$ of 0.05 of an overnight culture in LB complex medium with additional kanamycin (37 °C, 170 rpm). The standard incubation procedure included two phases. The first growth phase included 3 h at 37 °C, followed by 69 h at 15 °C to produce active

CatIBs. The optical density of the main cultures was determined to perform a normalization of the cell cultures to $\mathrm{OD}_{600\mathrm{nm}} \! = \! 10$ unless otherwise stated. The purification process was continued with 30 mL cell suspension with the specific optical density. The cells were harvested by centrifugation at 5,000 xg for 10 min (Beckman GS15-R, Beckman Coulter, Krefeld, Germany). The next centrifugation step (3 min at $5000 \times g$) was performed after washing the cell pellet with 20 mL of 0.9% NaCl solution. The supernatant was discarded. 2.7 mL cell lysis buffer, BugBuster® HT Protein Extraction Reagent (Merck KGaA, Darmstadt, Germany) with the addition of 0.146 g L^{-1} lysozyme, was added to the cell pellet to perform cell lysis. The suspension was incubated at 20 °C for 20 min and 750 rpm. After cell lysis the soluble and insoluble protein fraction were separated by centrifugation at 5000 xg for 30 min. The pellet was washed with 20 mL Milli-Q[®] water followed by centrifugation. 30 mL Milli-Q[®] water was added to the CatIB pellet and 1 mL aliquots in 1.5 mL Eppendorf tubes were made. A centrifugation step was performed and the supernatant was discarded (10,000 xg for 5 min). The pellets were used for enzyme assay or for weight determination. The CatIB weight was determined after drying the pellet at 80 °C for 24 h, followed by a second 24 h step in a desiccator. The enzymatic assay samples were stored on ice at 4 °C overnight and was used for enzyme activity measurements on the next day.

Sodium dodecyl sulfate-polyacrylamide gel electrophoresis (SDS-PAGE)

For SDS-PAGE analysis sample preparation was performed by adding $2\times \text{Laemmli}$ sample buffer to a purified CatIB-water suspension and to the soluble fraction originated from a cell culture with a normalized $\text{OD}_{600\text{nm}}$ of 10 (See Protein production, cell disruption and protein purification). After incubation for 10 min at 95 °C, the samples were applied to Criterion 4–12% Bis-Tris protein gel, 1.0 mm, with 18 wells (Bio-Rad Laboratories GmbH, Feldkirchen, Germany) together with a protein marker (PageRuler Prestained Protein *ladder*, ThermoFisher Scientific). Gel electrophoresis was performed in NuPAGE MES SDS running buffer (1x) at 200 V, 500 mA and 150 W. The gel was stained with Simply Blue SafeStain for 1 h.

Microscopic analysis

Phase-contrast microscopic analysis was performed for $E.\ coli$ BL21(DE3) strains with CatIB formation strains. 1 μL of each sample was given on a microscope slide and covered with a coverslip. The microscope slide was positioned upside down on the desk of an inverted Nikon Eclipse Ti2 microscope (Nikon GmbH, Düsseldorf,

Küsters et al. Microbial Cell Factories (2022) 21:108

Germany). The sample was observed with a CFI Plan Apo Lambda 100X Oil objective (Nikon GmbH, Düsseldorf, Germany) and images were taken with a Thorlab camera DCC154M-GL (Thorlabs Inc., Newton, New Jersey, USA). The amount of cells that carried CatIBs was counted by analyzing at least 50 cells per CatIB variant.

Activity assay

Enzyme activity testing was performed by adding 40 mM TAE buffer (pH 7), 200 mM glucose and 0.4 mM NAD⁺ to the CatIB pellet, originated from a cell culture with a normalized OD_{600nm} of 10 (See Protein production, cell disruption, and protein purification). The soluble fraction, after cell lysis, was refilled with TAE-glucose-NAD⁺ ratio compared to the CatIB pellet fraction. The samples were incubated at 1000 rpm and 37 °C. Samples were taken after 0, 3, 6, 12 and 20 min and the enzyme was inactivated by adding 80% (v/v) methanol. The inactivated samples were diluted 1:10 with 40 mM TAE buffer, before the NADH fluorescence was analyzed photometrically in an UV microtiter plate (pro infinite m200, Tecan, Männedorf, CH). NADH was measured with an excitation wavelength of 340 nm and an emission wavelength of 470 nm. A calibration curve of different NADH concentrations was measured with the same parameters.

Storage stability experiment

Four 100 mL main cultivations of E. coli BL21(DE3) with BsGDH-PT-CBDCell CatIBs were produced in 1 L shaking flasks. After cultivation, they were combined and the OD600nm was adjusted to a value of 10. The samples were purified with the same protocol as before (See protein production, cell disruption and protein purification). The first half of the purified CatIBs was divided in 1.5 mL reaction tubes with 1 mL CatIBs each with a following centrifugation step at 10,000 xg for 5 min. The supernatant was discarded, before the samples were stored at -20 °C as wet pellets (WP). The other half of the samples were first lyophilized at -54 °C and 0.01 mbar for 24 h before storing them at -20 °C as lyophilized pellets (LP). The reference samples (day 0) were tested via activity assay in triplicates (See activity assay) directly after purification. The storage stability of WP and LP were tested after 9, 17, 31, 39, 44 and 56 days at -20 °C (See activity assay).

NADH/CatlB recycling experiment

50 mL main cultivation of *E. coli* BL21(DE3) with *Bs*GDH-PT-CBDCell CatIBs were produced in 1 L shaking flasks. After cultivation they were adjusted to OD600nm 20. The samples were purified with the same protocol as before (See protein production, cell disruption and protein purification). The purified CatIBs were

divided in 1.5 mL reaction tubes with 1 mL CatIBs each. The activity of the CatIBs was tested in repetitive batches. While the CatIBs were reused for 11 cycles, 0.5 mL of the reaction solution, containing 40 mM TAE buffer (pH 7), 11.5 U ScADH (Sigma-Aldrich: A3263_150KU), 20 mM propanal, 200 mM glucose and 0.4 mM NAD⁺, were freshly added after each cycle. The reaction was performed for 30 min at 37 °C and 40 μ L samples were inactivated with 160 μ L methanol. The samples were prepared and NADH levels were measured as before (See activity assay). Moreover, the propanol concentration of the samples was analyzed via GC.

GC analysis

Samples were analyzed using a gas chromatograph (Thermo TRACE_1300_1310, Thermo Scientific, Waltham, USA) with a CP-Chirasil-Dex CB (Agilent, Santa Clara, USA) column (i.d. 0.25 mm; $25~\text{m}\times0.25~\mu\text{m}$), starting at 40 °C, hold for 0.5 min, followed by a gradient of 10 °C/min to 77 °C which was held for 0.75 min. Detection was done by FID with propanol showing a retention time of 4.13 min.

Abbreviations

ADH: Alcohol dehydrogenase; CatlB: Catalytically active inclusion body; GDH: Glucose dehydrogenase; P_v: Volumetric productivity; SDS-PAGE: Sodium dodecyl sulfate polyacrylamide gel electrophoresis.

Supplementary Information

The online version contains supplementary material available at https://doi.org/10.1186/s12934-022-01816-2.

Additional file 1: Table S1: Plasmids used in this study. Table S2: Recipe of M9 Autoinduction medium—1000 mL Figure S1: Evaluation of CatlB formation by SDS-PAGE analysis. After cultivation, the optical density of the cultures were normalized to OD600nm = 10. The cells were disrupted and the crude cell extract was separated by centrifugation into the soluble and the insoluble CatlB-containing pellet fraction. The pellet fraction was washed with Milli-Q water. The pellet samples were 1:1 diluted with SDS sample buffer and 15 μ L of each samples was loaded onto the gel. The gel was stained with SimplyBlue[™] SafeStain.

Acknowledgements

This work was funded by the state of North Rhine Westphalia (NRW) and the European Regional Development Fund (EFRE), Project "CLIB-Kompetenzzentrum Biotechnologie (CKB)" 34.EFRE-0300097 and by the Deutsche Forschungsgemeinschaft (DFG, German Research Foundation) under Germany's Excellence Strategy — Exzellenzcluster 2186 "The Fuel Science Center" ID: 390919832. Open Access publication was funded by the Deutsche Forschungsgemeinschaft (DFG, German Research Foundation)—491111487.

Author contributions

KK performed NADH/CatlB recycling, planned and analyzed all experiments and wrote the manuscript. RS did the strain construction, enzyme purification and analysis of 14 BsGDH variants. CW established workflows for CatlB storage stability and recycling experiments. RH performed CatlB storage stability experiment. JDS performed GC analysis and helped to finalize the manuscript. WW helped to finalize the manuscript.

Küsters et al. Microbial Cell Factories

(2022) 21:108

and supervised the entire project. All authors read and approved the final manuscript.

Funding

Open Access funding enabled and organized by Projekt DEAL. This work was funded by the state of North Rhine Westphalia (NRW) and the European Regional Development Fund (EFRE), Project "CLIB-Kompetenzzentrum Biotechnologie (CKB)" 34.EFRE-030097 and by the Deutsche Forschungsgemeinschaft (DFG, German Research Foundation) under Germany's Excellence Strategy — Exzellenzcluster 2186 "The Fuel Science Center" ID: 390919832. Open Access publication was funded by the Deutsche Forschungsgemeinschaft (DFG, German Research Foundation)-491111487.

Availability of data and materials

All data generated or analyzed during this study are included in this article and its Additional file 1.

Declarations

Ethics approval and consent to participate

Not applicable.

Consent for publication

Not applicable.

Competing of interests

The authors declare that they have no competing interest.

Author details

¹Institute of Bio- and Geosciences IBG-1: Biotechnology, Forschungszentrum Jülich GmbH, 52425 Jülich, Germany. ²Institute of Biotechnology, RWTH Aachen University, 52074 Aachen, Germany. ³Aachen Biology and Biotechnology (ABBt), RWTH Aachen University, 52074 Aachen, Germany. ⁴Computational Systems Biotechnology (AVT.CSB), RWTH Aachen University, 52074 Aachen, Germany.

Received: 4 April 2022 Accepted: 9 May 2022 Published online: 02 June 2022

References

- Kloss R, Limberg MH, Mackfeld U, Hahn D, Grünberger A, Jäger VD, et al. Catalytically active inclusion bodies of L-lysine decarboxylase from *E coli* for 1,5-diaminopentane production. Sci Rep. 2018;8:5856. https://doi.org/ 10.1038/s41598-018-24070-2.
- Jäger VD, Lamm R, Küsters K, Ölçücü G, Oldiges M, Jaeger K-E, et al. Catalytically-active inclusion bodies for biotechnology-general concepts, optimization, and application. Appl Microbiol Biotechnol. 2020;104:7313– 29. https://doi.org/10.1007/s00253-020-10760-3.
- Krauss U, Jäger VD, Diener M, Pohl M, Jaeger K-E. Catalytically-active inclusion bodies-Carrier-free protein immobilizates for application in biotechnology and biomedicine. J Biotechnol. 2017;258:136–47. https:// doi.org/10.1016/j.jbiotec.2017.04.033.
- Küsters K, Pohl M, Krauss U, Ölçücü G, Albert S, Jaeger K-E, et al. Construction and comprehensive characterization of an *Ec*LDCc-CatlB set-varying linkers and aggregation inducing tags. Microb Cell Fact. 2021;20:1–12. https://doi.org/10.1186/s12934-021-01539-w.
- Kamel S, Walczak MC, Kaspar F, Westarp S, Neubauer P, Kurreck A. Thermostable adenosine 5'-monophosphate phosphorylase from *Thermo*coccus kodakarensis forms catalytically active inclusion bodies. Sci Rep. 2021;11:1–9. https://doi.org/10.1038/s41598-021-96073-5.
- Lin Z, Zhou B, Wu W, Xing L, Zhao Q. Self-assembling amphipathic alpha-helical peptides induce the formation of active protein aggregates in vivo. Faraday Discuss. 2013;166:243–56. https://doi.org/10.1039/c3fd0 0068k.
- Jäger VD, Lamm R, Kloß R, Kaganovitch E, Grünberger A, Pohl M, et al. A synthetic reaction cascade implemented by colocalization of two proteins within catalytically active inclusion bodies. ACS Synth Biol. 2018;7:2282–95. https://doi.org/10.1021/acssynbio.8b00274.

- Jäger VD, Kloss R, Grünberger A, Seide S, Hahn D, Karmainski T, et al. Tailoring the properties of (catalytically)-active inclusion bodies. Microb Cell Fact. 2019;18:1–19. https://doi.org/10.1186/s12934-019-1081-5.
- Weckbecker A, Hummel W. Glucose Dehydrogenase for the Regeneration of NADPH and NADH. In: Barredo JL, editor. Microbial Enzymes and Biotransformations. Totowa, NJ: Humana Press; 2005. p. 225–38. https://doi.org/10.1385/1-59259-846-3:225.
- Hansen RL, Schwinden MD, Banerjee A, Brzozowski DB, Chen B-C, Patel BP, et al. Enzymatic Synthesis of L-6-hydroxynorleucine. Bioorg Med Chem. 1999;7:2247–52. https://doi.org/10.1016/S0968-0896(99)00158-3.
- Lin S-S, Miyawaki O, Nakamura K. Continuous production of I-carnitine with NADH regeneration by a nanofiltration membrane reactor with coimmobilized I-carnitine dehydrogenase and glucose dehydrogenase. J Biosci Bioeng. 1999;87:361–4. https://doi.org/10.1016/S1389-1723(99) 80046-2
- Peschke T, Bitterwolf P, Gallus S, Hu Y, Oelschlaeger C, Willenbacher N, et al. Self-assembling all-enzyme hydrogels for flow biocatalysis. Angew Chem Int Ed Engl. 2018;57:17028–32. https://doi.org/10.1002/anie.20181 0331.
- Diener M, Kopka B, Pohl M, Jaeger K-E, Krauss U. Fusion of a coiledcoil domain facilitates the high-level production of catalytically active enzyme inclusion bodies. ChemCatChem. 2016;8:142–52. https://doi.org/ 10.1002/cctc.201501001.
- Zhou B, Xing L, Wu W, Zhang X-E, Lin Z. Small surfactant-like peptides can drive soluble proteins into active aggregates. Microb Cell Fact. 2012;11:10. https://doi.org/10.1186/1475-2859-11-10.
- Wang X, Zhou B, Hu W, Zhao Q, Lin Z. Formation of active inclusion bodies induced by hydrophobic self-assembling peptide GFIL8. Microb Cell Fact. 2015;14:88. https://doi.org/10.1186/s12934-015-0270-0.
- Jong WSP, Vikström D, Houben D, van Berg Saparoea HB, de Gier J-W, Luirink J. Application of an *E coli* signal sequence as a versatile inclusion body tag. Microb Cell Fact. 2017. https://doi.org/10.1186/ s12934-017-0662-4.
- Choi S-L, Lee SJ, Ha J-S, Song JJ, Rhee YH, Lee S-G. Generation of catalytic protein particles in *Escherichia coli* cells using the cellulose-binding domain from *Cellulomonas fimi* as a fusion partner. Biotechnol Bioproc E. 2011;16:1173–9. https://doi.org/10.1007/s12257-011-0336-8.
- Xing L, Wu W, Zhou B, Lin Z. Streamlined protein expression and purification using cleavable self-aggregation tags. Microb Cell Fact. 2011;10:1–7. https://doi.org/10.1186/1475-2859-10-42.
- Kloss R, Karmainski T, Jäger VD, Hahn D, Grünberger A, Baumgart M, et al. Tailor-made catalytically active inclusion bodies for different applications in biocatalysis. Catal Sci Technol. 2018;8:5816–26. https://doi.org/10.1039/ C8CY018911
- Sunitha K, Chung BH, Jang KH, Song KB, Kim CH, Rhee SK. Refolding and purification of *Zymomonas mobilis* levansucrase produced as inclusion bodies in fed-batch culture of recombinant *Escherichia coli*. Protein Expr Purif. 2000;18:388–93. https://doi.org/10.1006/prep.2000.1204.
- 21. Wu W, Xing L, Zhou B, Lin Z. Active protein aggregates induced by terminally attached self-assembling peptide ELK16 in *Escherichia coli*. Microb Cell Fact. 2011;10:1–8. https://doi.org/10.1186/1475-2859-10-9.
- Miyazaki K. Lethal ccdB gene-based zero-background vector for construction of shotgun libraries. J Biosci Bioeng. 2010;110:372–3. https://doi. org/10.1016/j.jbiosc.2010.02.016.

Publisher's Note

Springer Nature remains neutral with regard to jurisdictional claims in published maps and institutional affiliations.